DOI: 10.21062/mft.2025.078 http://www.journalmt.com

Tensile Behaviour of Zn–Mg Heterostructured Materials for Biodegradable Implant Applications

Anna Boukalová (0009-0008-9035-4182)*[1], David Nečas (0000-0002-5995-5181)[1], Drahomír Dvorský (0000-0001-8629-8407)[2], Jan Šťovíček (0009-0005-8312-9655)[1], Jan Pokorný (0009-0009-5851-8447)[1], Jiří Kubásek (0000-0001-6008-0127)[1]
[1]Department of Metals and Corrosion Engineering, University of Chemistry and Technology, Technická 6, Prague 6, 166 28, Czech Republic. *E-mail: boukaloa@vscht.cz
[2] Department of Physics, Czech Academy of Science, Na Slovance 1999/2, Prague 8, 182 21, Czech Republic, E-mail: dvorsky@fzu.cz

Biodegradable zinc-based alloys have recently attracted attention as promising candidates for temporary implant applications due to their favourable corrosion behaviour and biocompatibility. In this study, three materials — pure Zn, Zn–1Mg alloy, and a Zn + Zn–1Mg composite — were fabricated via powder metallurgy and extrusion to evaluate their microstructural characteristics and tensile performance. The composite material was designed to combine ductile Zn regions with a reinforcing Zn–1Mg network, aiming to achieve a balance of strength and ductility. Microstructural analysis revealed coarse-grained Zn regions surrounded by ultrafine-grained Zn–1Mg areas containing Mg_2Zn_{11} particles, with oxide particles present at the Zn/Zn–1Mg interfaces. Tensile testing showed improvement in mechanical performance compared to the individual constituents.

Keywords: Zinc Alloys, Heterostructure, Biodegradable, Microstructure, Tensile Properties

1 Introduction

Biodegradable metallic implants have emerged as a novel solution to the limitations of traditional permanent medical devices. By gradually dissolving within the body after fulfilling their function, these materials can eliminate the need for secondary removal surgeries, reducing patient discomfort, lowering healthcare costs, and minimising surgical risks. Among the candidate materials, zinc-based alloys have emerged as promising alternatives to magnesium- and iron-based systems due to their moderate corrosion rate, essential role in human metabolism, and favourable biocompatibility. However, the low strength and limited ductility of pure zinc remain critical limitations for orthopaedic applications, where implants must withstand substantial stresses during the healing process [1-5]. Alloying zinc with magnesium has been shown to enhance mechanical properties through solid solution strengthening and precipitation hardening, while also enhancing biocompatibility and corrosion behaviour [6-8].

Beyond alloy composition, microstructural design plays a critical role in balancing strength, ductility, and corrosion resistance. Recent advances in severe plastic deformation techniques, such as mechanical milling and powder consolidation, have enabled the development of materials with a harmonic structure [9, 10]. This type of heterostructured material is characterised by a continuous network of fine-grained 3D skeleton surrounding coarse-grained cores [10]. Due to hetero-deformation-induced strengthening initiated during deformation of this microstructural architecture, an advantageous combination of high strength and improved ductility is reached by promoting strain partitioning, work hardening capacity and delaying the onset of localised deformation [11-14].

Given that implants are often subjected to tensile stresses in service, a thorough understanding of how Zn–Mg harmonic structured alloys behave under tensile loading is essential for predicting in vivo performance and ensuring mechanical reliability throughout the degradation process [15-17].

This work aims to evaluate the tensile behaviour of Zn–Mg hetero-structured materials. By correlating mechanical performance with the microstructural features, this study provides insights into the design and optimisation of biodegradable metallic implants with tailored strength and ductility.

2 Experiment

2.1 Mechanical alloying

Mechanically alloyed Zn-1Mg powder was prepared using the Retsch E-max mill with ZrO_2 milling vessels and 1 cm diameter ZrO_2 milling balls. The milling was carried out in an argon atmosphere for 4 hours at 800 RPM, with the direction of rotation changing every 10 minutes. The mass ratio of milled powder to milling balls was 1:5.

2.2 Consolidation and extrusion

Before consolidation, <45 μm particles of Zn-1Mg were mixed with 63-100 μm particles of pure zinc (50:50 wt. %) in a turbula. This prepared mixture was then consolidated using a spark plasma sintering machine (FCT Systeme HP-D 10) under an argon atmosphere at set parameters: 300°C, 10 min, 80 MPa and subsequently extruded at 200°C with an extrusion ratio of 10 and a speed of 0.2 mm/s. The controlling materials of pure zinc and Zn-1Mg were prepared under the same preparation processes.

2.3 Microstructure

Materials were ground using SiC papers P240-P400 and subsequently polished by a D2 diamond polishing paste (URdiamant) and Eposil Non-Dry suspension (QATM). The microstructure was studied by optical microscopy (Nikon Eclipse MA200 using NIS Elements software) and scanning electron microscopy (Tescan Lyra 3) equipped with an EDX Analyser (Oxford Instruments AZTec). The phase composition was further studied by X-ray diffraction (PANanalytical X'Pert3 with a Cu anode – λ = 1.5406 Å) using HighScore Plus and Topas 3 software. The grain size and size of the present phases were evaluated by image analysis in the ImageJ software.

2.4 Mechanical properties

The tensile tests were performed using the Instron 8872 machine on samples of specified dimensions (Fig. 1). These tests were performed at 25 °C at a strain rate of 1.5 mm/min with three samples of each material.

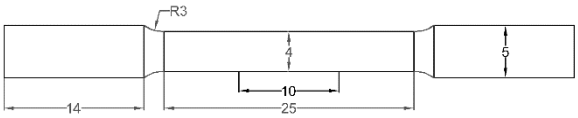

Fig. 1 *Dimensions of the sample for tensile testing*

2.5 Corrosion resistance

All electrochemical measurements were performed in a conventional three-electrode setup (working electrode: our sample, reference electrode: Ag/AgCl (ACLE) - 3 mol/l, counter electrode: glassy graphite) using a Gamry Instruments electrochemical workstation (Gamry Reference 600). The volume of electrolyte per area was 190 mL·cm^{-2}. Samples were first ground on SiC paper P2500 to achieve reproducible surfaces. The anodic polarisation curves were recorded in a physiological solution (9 g/l NaCl) of pH 6 at 25 °C, aerated for 10 minutes, with 2 h stabilisation of open circuit potential (E_{oc}). The potential was measured with respect to the value of ACLE. The start of cyclic polarisation started at a potential -50 mV/E_{oc}, was reversed at 1 mA/cm^2 and continued to -50mV/E_{oc}. The scan rate was 1 mV/s.

3 Results and discussion

3.1 Microstructure

The microstructure of sintered and extruded pure zinc (Fig. 2) consisted of the initial powder particles with partially disrupted oxide shells along the original powder surface. The disruption took place during extrusion from oxide layers originally present on the initial powder particles due to exposure to oxygen in the air. White arrows show examples of these. In some cases, originating oxide particles can be agglomerated into bigger clusters due to the tendency to lower surface energy. Similarly, these were also observed in other zinc alloys prepared by a combination of powder metallurgy and extrusion [7, 18]. The observed zinc grains were of 5-20 μm in size.

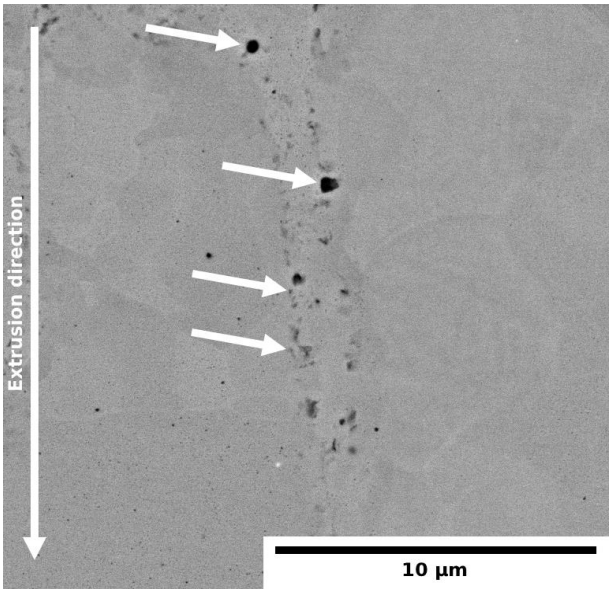

Fig. 2 *The microstructure of extruded Zn*

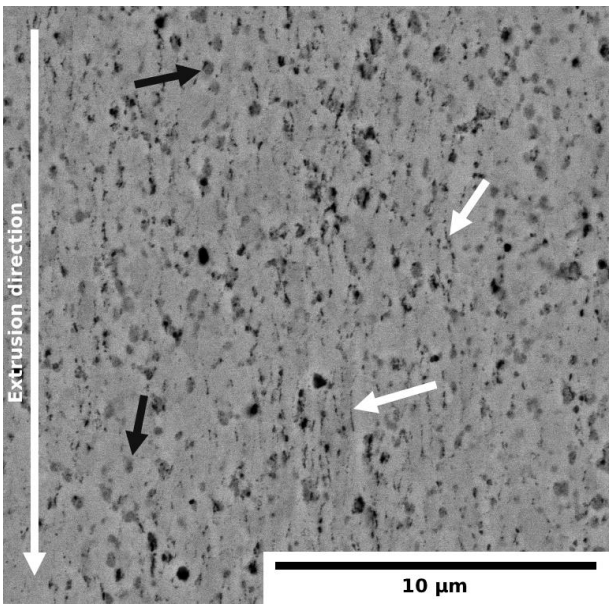

Fig. 3 *The microstructure of extruded Zn-1Mg*

The microstructure of the compacted Zn–1Mg alloy shown in Fig. 3 consisted of zinc grains (300-700 nm) and Mg_2Zn_{11} intermetallic phases (200-400 nm) pointed by blue arrows. Energy-dispersive X-ray (EDX) analysis in the scanning electron microscope (SEM) indicated that the solid solution of zinc contained 0.6 wt.% magnesium. According to the XRD analysis, the content of the Mg_2Zn_{11} phase is equal to ~7 wt.%. Magnesium and zinc oxides were also detected in the volume of the material (white arrows). This is in agreement with the work by Kubásek et al., who similarly studied extruded Zn-1Mg material [18].

The Zn+Zn-1Mg material's microstructure (Fig. 4) was composed of distinguished areas of pure zinc with coarse grains (3-18 μm) and the Zn-1Mg alloy with fine grains (300-600 nm). These areas are deformed in the direction of extrusion. The area of Zn-1Mg alloy was formed by the solid solution of zinc and the Mg_2Zn_{11} phase of 150-400 nm (blue arrows). According to the XRD analysis, the content of the Mg_2Zn_{11} phase was <1 wt. %. However, this result can be influenced by the size of this phase and the detection limit of the XRD method. Zinc and magnesium oxide particles were detected on the interface of these two areas and also in the area of Zn-1Mg alloy (white arrows).

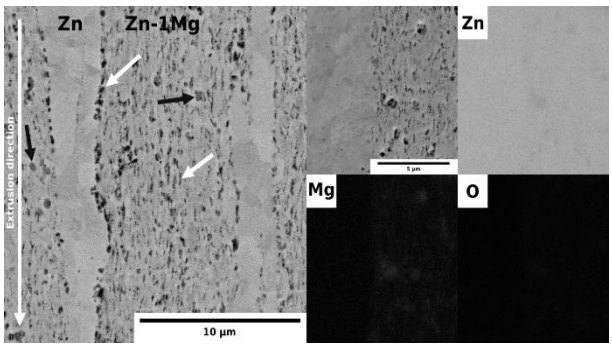

Fig. 4 *The microstructure of extruded Zn+Zn-1Mg*

3.2 Tensile test

The tension testing process (Tab. 1) revealed that the Zn+Zn-1Mg material behaves like a mixture of individual components. The addition of Zn-1Mg increased the strength by almost 200 MPa compared to pure zinc. As for ductility, although it decreased compared to pure zinc, it remains very favourable at 13%, compared to the Zn-1Mg alloy at 5%.

Tab. 1 *Tensile test results*

	Yield strength [MPa]	Ultimate tensile strength [MPa]	Elongation to failure [%]
Zn	109 ± 7	145 ± 1	19 ± 4
Zn-1Mg	217 ± 19	403 ± 7	5 ± 2
Zn+Zn-1Mg	251 ± 7	333 ± 7	13 ± 2

The Zn+Zn-1Mg material exhibited improved mechanical properties compared to its individual constituents. It is important to mention that the mechanical properties of the Zn+Zn-1Mg at 0.5 net weight % surpass those of materials with the same chemical composition prepared by extrusion [19, 20]. However, based on these results, it is likely that no effective load transfer and desired interaction between the soft zinc domains and the harder Zn–1Mg domains has occurred. This behaviour can be primarily attributed to the presence of oxide particles. These particles, which are formed during extrusion from oxide shells typically formed during powder production and handling, can act as physical barriers at the particle interfaces.

To further analyse the possible adverse impact of the oxide particles, we observed the surface of a fracture plane, both in cross-section and longitudinal section.

Fractographic analysis of pure zinc after tensile testing (Fig. 5) revealed a predominantly ductile fracture mechanism. At low magnification, the fracture surface exhibited a fibrous morphology with elongated grains, indicating distributed plastic deformation. Higher magnification observations revealed fine, equiaxed dimples characteristic of a void nucleation–growth–coalescence process. These voids likely nucleated at grain boundaries or mentioned oxide particles, where local stress concentrations facilitated crack initiation. The absence of cleavage facets or intergranular separation confirms that brittle fracture was not a significant factor. This behaviour is consistent with the high deformability of zinc, where dislocation motion accommodates plastic strain until failure occurs through microvoid coalescence.

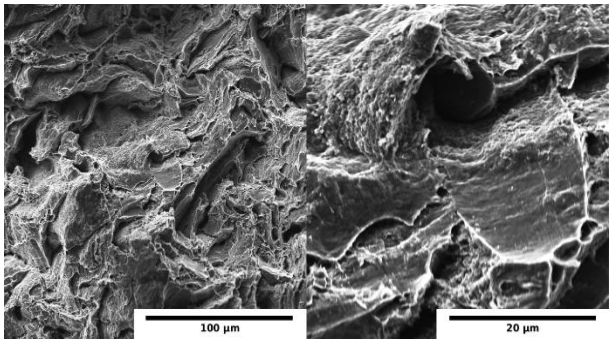

Fig. 5 *Cross-section fracture planes of Zn*

The tensile fracture of the Zn–1Mg alloy shown in Fig. 6 exhibited predominantly brittle characteristics, as evidenced by the cleavage-like facets and intergranular features observed on the fracture surface. At higher magnifications, the fracture plane revealed sharp steps and microcracks without evidence of ductile dimpling, suggesting limited plastic deformation before failure. Crack initiation is likely associated with stress concentration at oxide shells on grain boundaries and Mg_2Zn_{11} phases, which act as preferential sites for decohesion. Subsequent crack propagation occurred rapidly along grain boundaries and cleavage planes, leading to a mixed intergranular and quasi-cleavage fracture mode. The presence of these brittle features indicates that alloying with Mg reduces the overall plasticity of the material compared to pure Zn, primarily due to the formation of hard and brittle secondary phases.

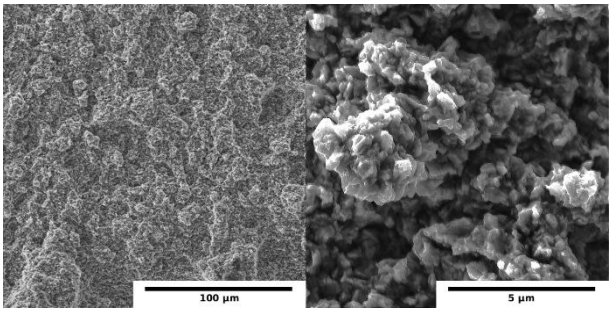

Fig. 6 *Cross-section fracture planes of Zn-1Mg*

In Fig. 7, the fracture surface of Zn+Zn-1Mg material revealed a clear contrast between pure Zn and the Zn–1Mg. Whereas the pure Zn region exhibited a ductile fracture mode, the Zn–1Mg alloy showed a brittle fracture appearance with cleavage-like facets and intergranular features, indicating rapid crack propagation with limited plastic deformation. The fracture of the Zn + Zn–1Mg material did not follow a preferential crack-growth path but propagated through both the pure Zn and Zn–1Mg regions indiscriminately, with no areas being bypassed during crack advance, as can be seen in Fig. 8. The absence of any ductile–brittle transition across the fracture surface suggests that the material behaves as a mechanical mixture rather than a synergistic composite. Furthermore, voids were observed at the interfaces of different zones and throughout the volume of the Zn-1Mg alloy.

The lack of synergy can be attributed to the presence of oxide particles located at the Zn/Zn–1Mg interface. Even though the crack did not propagate preferentially along the interface. Its presence is the most likely reason why synergy between the individual regions could not occur, and the material therefore behaves only as a mixture of individual areas. Therefore, substantial hetero-deformation-induced reinforcement and hardening did not occur significantly. Similar voids were also observed in the work of Sojitthamporn et al. [21], who observed the fracture mechanism of Cu harmonic structure. According to their work, at first, as strain increases, voids grow mainly in the shell and interface areas. Crack propagation is partially hindered in the ductile core, which helps preserve overall ductility. At higher strain, however, the structure can no longer sustain the applied load, leading to crack coalescence throughout the material and final fracture. They also suggested that these voids may originate from the high diversity of the regions' mechanical properties [21].

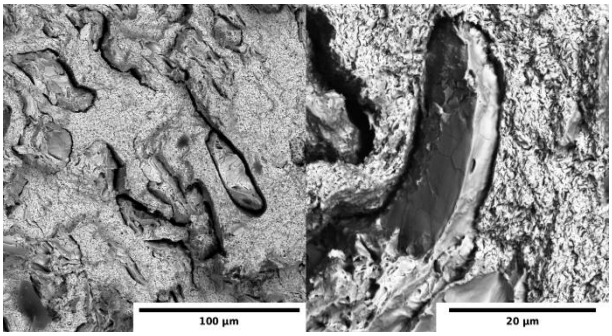

Fig. 7 *Cross-section fracture planes of Zn+Zn-1Mg*

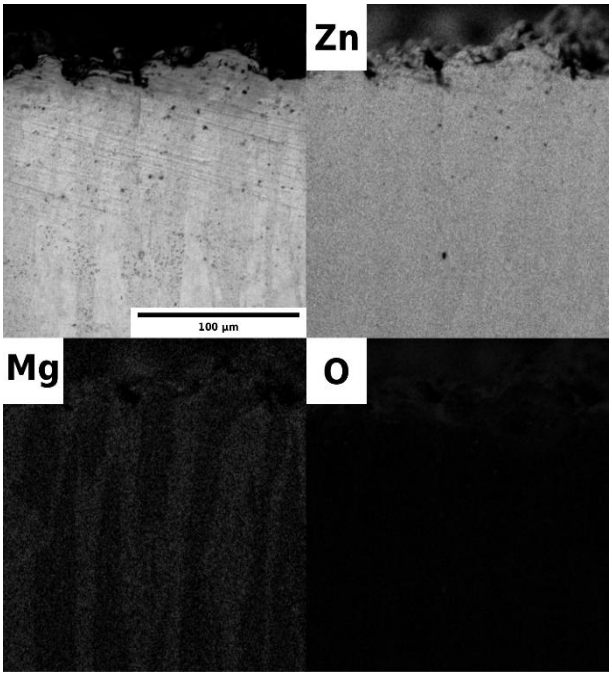

Fig. 8 *Longitudinal section fracture planes of Zn+Zn-1Mg*

4 Corrosion resistance

To further investigate the potential use of this material as a biodegradable implant, cyclic polarisation measurements were performed in physiological solution. As shown in the polarisation curves in Fig. 9 and in Tab. 2, the open-circuit potentials of all three investigated conditions, pure Zn, Zn–1Mg, and the Zn + Zn-1Mg harmonic-structure material, lie within a narrow potential range. Likewise, the corresponding

corrosion current densities derived from the near region are comparable, indicating similar baseline corrosion kinetics.

Consequently, based on these cyclic polarisation results, there is no evidence that the harmonic-structure design has a detrimental effect on the corrosion response of the zinc-based material in physiological solution. Rather, its electrochemical performance remains comparable to that of pure Zn.

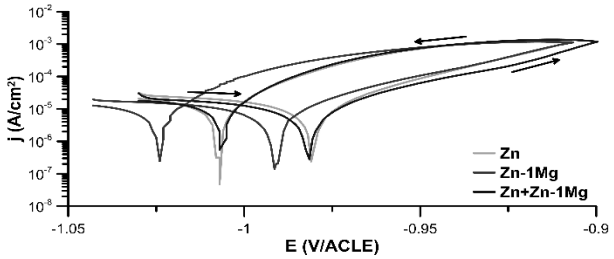

Fig. 9 *Cyclic polarisation tests*

Tab. 2 *Electrochemical parameters derived from potentiodynamic curves*

	E_{OC} [V/ACLE]	v_{corr} [mm/year]
Zn	-0.981	0.07
Zn-1Mg	-0.991	0.06
Zn+Zn-1Mg	-0.982	0.07

However, the measured corrosion rates remain significantly lower than the levels generally considered necessary for biodegradable implants, which are expected to degrade at approximately 0.5 mm/year [22]. This indicates that, despite its stability, the zinc-based material may corrode too slowly to meet the required degradation profile for temporary biomedical devices.

5 Conclusion

In this work, three materials, namely Zn, Zn-1Mg and Zn+Zn-1Mg, were prepared by powder metallurgy and extrusion. The composite of Zn and Zn-1Mg was tested as a candidate material for biodegradable implant utilisation. Therefore, a thorough analysis is required to evaluate the dependence of microstructure on the behaviour of the material under tensile loading.

Microstructural characterisation revealed that the Zn+Zn–1Mg composite exhibits a harmonic structure, consisting of coarse-grained Zn cores surrounded by a Zn–1Mg alloy network. The Zn–1Mg regions contained fine grains in the order of hundreds of nanometres and Mg_2Zn_{11} intermetallic particles, while oxide particles were observed at the interfaces between the two phases.

Mechanical testing demonstrated that the combination of Zn and Zn–1Mg leads to a significant increase in yield strength compared to pure Zn, while partially retaining ductility. However, the expected full synergy was not completely achieved, likely due to the presence of oxide particles and differences in deformation behaviour between the shell and core regions. Fractographic analysis indicated a complex fracture mechanism involving both interfacial decohesion and microvoid coalescence.

The cyclic polarisation measurements demonstrated that the harmonic-structure design does not negatively influence the electrochemical behaviour of the zinc-based material, as all tested conditions exhibited comparable values and corrosion current densities. Nevertheless, the overall corrosion rates remain below the degradation rate of approximately 0.5 mm·year^{-1} required for biodegradable implant applications.

Overall, the results highlight that tailoring the morphology and interfacial quality of the Zn–Zn–1Mg system is crucial for optimising mechanical performance. By minimising oxide formation and refining the connectivity of the Zn–1Mg network, further improvements in strength–ductility balance may be achieved. These findings contribute to a better understanding of microstructure–property relationships in Zn-based harmonic materials.

Acknowledgement

This research was supported by the Czech Science Foundation (project no. 21–11439K) and by the project "Mechanical Engineering of Biological and Bio-inspired Systems", funded as project No. CZ.02.01.01/00/22_008/0004634 by Programme Johannes Amos Comenius, call Excellent Research. This research was also supported by the Czech Science Foundation (project no. 25-16144S). We also thank the Specific university research, project A1_FCHT_2025_011 and A2_FCHT_2025_046.

Data availability

The data used within the manuscript can be accessed through Zenodo link: https://doi.org/10.5281/zenodo.17751768.

References

[1] KUBÁSEK, J.; VOJTĚCH, D. (2012). Zn-based alloys as an alternative biodegradable materials. In: *Proc. Metal*, Vol. 5, 23-25.

[2] VOJTECH, D.; KUBASEK, J.; SERAK, J.; NOVAK, P. (2011). Mechanical and corrosion properties of newly developed biodegradable Zn-based alloys for bone fixation. In: *Acta Biomater*, Vol. 7, 9, 3515-3522.

[3] LOVAŠI, T.; PINC, J.; VOŇAVKOVÁ, I. (2019). Zinc-based Degradable Biomaterials - Limitations and Enhancements. In: *Manufacturing Technology*, Vol. 19, 4, 632-636.

[4] DVORSKÝ, D.; KUBÁSEK, J.; VOJTĚCH, D. (2020). Microstructure, mechanical and corrosion properties of extruded milled magnesium powder. In: *Manufacturing Technology*, Vol. 20, 6, 708-713.

[5] VOJTĚCH, D.; KUBÁSEK, J.; VODĚROVÁ, M. (2012). Structural, mechanical and in vitro corrosion characterization of as-cast magnesium based alloys for temporary biodegradable medical implants. In: *Manufacturing technology*, Vol. 12, 13, 285-292.

[6] KUBÁSEK, J.; DVORSKÝ, D.; ČAPEK, J.; MARKÉTA, S.; KLÁRA, H.; VOJTĚCH, D. (2020). Zinc alloys as prospective materials for biodegradable medical devices. In: *Manufacturing Technology*, Vol. 20, 6, 779-784.

[7] NEČAS, D.; HYBÁŠEK, V.; PINC, J.; ŠKOLÁKOVÁ, A.; VOŇAVKOVÁ, I.; HOSOVÁ, K.; ZLÁMAL, M.; BOUKALOVÁ, A.; POKORNÝ, J.; DVORSKÝ, D.; et al. (2024). Exploring the microstructure, mechanical properties, and corrosion resistance of innovative bioabsorbable Zn-Mg-(Si) alloys fabricated via powder metallurgy techniques. In: *Journal of Materials Research and Technology*, Vol. 29, 3626-3641.

[8] SHI, Z. Z.; GAO, X. X.; ZHANG, H. J.; LIU, X. F.; LI, H. Y.; ZHOU, C.; YIN, Y. X.; WANG, L. N. (2020). Design biodegradable Zn alloys: Second phases and their significant influences on alloy properties. In: *Bioact Mater*, Vol. 5, 2, 210-218.

[9] SHOKRY, A.; AHADI, A.; STAHLE, P.; ORLOV, D. (2021). Improvement of structural efficiency in metals by the control of topological arrangements in ultrafine and coarse grains. In: *Sci Rep*, Vol. 11, 1, 17445.

[10] AMEYAMA, K.; CAZES, F.; COUQUE, H.; DIRRAS, G.; KIKUCHI, S.; LI, J.; MOMPIOU, F.; MONDAL, K.; ORLOV, D.; SHARMA, B.; et al. (2022). Harmonic structure, a promising microstructure design. In: *Materials Research Letters*, Vol. 10, 7, 440-471.

[11] PARK, H. K.; AMEYAMA, K.; YOO, J.; HWANG, H.; KIM, H. S. (2018). Additional hardening in harmonic structured materials by strain partitioning and back stress. In: *Materials Research Letters*, Vol. 6, 5, 261-267.

[12] VAJPAI, S. K.; OTA, M.; ZHANG, Z.; AMEYAMA, K. (2016). Three-dimensionally gradient harmonic structure design: an integrated approach for high performance structural materials. In: *Materials Research Letters*, Vol. 4, 4, 191-197.

[13] ZHU, Y.; AMEYAMA, K.; ANDERSON, P. M.; BEYERLEIN, I. J.; GAO, H.; KIM, H. S.; LAVERNIA, E.; MATHAUDHU, S.; MUGHRABI, H.; RITCHIE, R. O.; et al. (2020). Heterostructured materials: superior properties from hetero-zone interaction. In: *Materials Research Letters*, Vol. 9, 1, 1-31.

[14] ZHU, Y.; WU, X. (2023). Heterostructured materials. In: *Progress in Materials Science*, Vol. *131*,

[15] RHO, J. Y.; KUHN-SPEARING, L.; ZIOUPOS, P. (1998). Mechanical properties and the hierarchical structure of bone. In: *Medical engineering & physics*, Vol. 20, 2, 92-102.

[16] CHANDRA, G.; PANDEY, A. (2020). Biodegradable bone implants in orthopedic applications: a review. In: *Biocybernetics and Biomedical Engineering*, Vol. 40, 2, 596-610.

[17] WEILER, A.; HOFFMANN, R. F.; STÄHELIN, A. C.; HELLING, H. J.; SÜDKAMP, N. P. (2000). Biodegradable Implants in Sports Medicine The Biological Base. In: *Arthroscopy: The Journal of Arthroscopic & Related Surgery*, Vol. 16, 3, 305-321.

[18] KUBÁSEK, J.; TORKORNOO, S.; NEČAS, D.; MCCARROLL, I.; HYBÁŠEK, V.; GAULT, B.; JABLONSKÁ, E.; DONIK, Č.; PAULIN, I.; GOGOLA, P.; et al. (2025). Towards increased strength and retained ductility of Zn–Mg-(Ag) materials for medical devices by adopting powder metallurgy processing routes. In: *Journal of Materials Research and Technology*, Vol. 37, 4345-4361.

[19] MOSTAED, E.; SIKORA-JASINSKA, M.; MOSTAED, A.; LOFFREDO, S.; DEMIR, A. G.; PREVITALI, B.; MANTOVANI, D.; BEANLAND, R.; VEDANI, M. (2016). Novel Zn-based alloys for biodegradable stent applications: Design, development and in vitro degradation. In: *J Mech Behav Biomed Mater*, Vol. 60, 581-602.

[20] WANG, L.-Q.; REN, Y.-P.; SUN, S.-N.; ZHAO, H.; LI, S.; QIN, G.-W. (2017). Microstructure, Mechanical Properties and Fracture Behavior of As-Extruded Zn–Mg Binary Alloys. In: *Acta Metallurgica Sinica (English Letters)*, Vol. 30, 10, 931-940.

[21] SOJITHAMPORN, P.; SAWANGRAT, C.; LEKSAKUL, K.; SHARMA, B.; AMEYAMA, K. (2022). Optimization of Mechanical Milling Process Parameters on Mechanical Properties and Fracture Mechanism of Harmonic-Structure Pure Cu. In: *Materials* Vol. 15, 23,

[22] VENEZUELA, J.; DARGUSCH, M. S. (2019). The influence of alloying and fabrication techniques on the mechanical properties, biodegradability and biocompatibility of zinc: A comprehensive review. In: *Acta Biomater*, Vol. 87, 1-40.